Amido-Bridged Cu_2N_2 Diamond Cores that Minimize Structural Reorganization and Facilitate Reversible Redox Behavior between a Cu^1Cu^1 and a Class III Delocalized $Cu^{1.5}Cu^{1.5}$ Species

Seth B. Harkins and Jonas C. Peters*

*Contribution from the Division of Chemistry and Chemical Engineering,
Arnold and Mabel Beckman Laboratories of Chemical Synthesis,
California Institute of Technology, Pasadena, California 91125*

Received July 17, 2003; E-mail: jpeters@caltech.edu

Abstract: A novel Cu_2N_2 diamond core structure supported by an $[SNS]^-$ ligand (**1**) ($[SNS]^-$ = bis(2-*tert*-butylsulfanylphenyl)amido) has been prepared. This dicopper system exhibits a fully reversible one-electron redox process between a reduced Cu^1Cu^1 complex, $\{[SNS][Cu]\}_2$ (**2**), and a class III delocalized $Cu^{1.5}Cu^{1.5}$ state, $[\{[SNS][Cu]\}_2][B(3,5-(CF_3)_2C_6H_3)_4]$ (**3**). Structural snapshots of both redox forms have been obtained to reveal remarkably little overall structural reorganization. The Cu···Cu bond distance nonetheless undergoes an appreciable compression (~0.13 Å) upon oxidation, providing a Cu···Cu distance of 2.4724(4) Å in the mixed-valence state that is virtually identical to the Cu···Cu distance observed in the reduced form of the Cu_A site of thiolate-bridged cytochrome *c* oxidase. Despite the low structural reorganization evident between **2** and **3**, the $[SNS]^-$ ligand is quite flexible. For example, square-planar geometries can prevail for divalent copper ions supported by $[SNS]^-$ as evident from the crystal structure of [SNS]CuCl (**4**). Physical characterization for the mixed valence complex **3** includes electrochemical, magnetic (SQUID), EPR, and optical data. The complex has also been examined by density functional methods. An attempt was made to measure the rate of electron self-exchange k_s between the Cu^1Cu^1 and the $Cu^{1.5}Cu^{1.5}$ complexes **2** and **3** by NMR line-broadening analysis in dichloromethane solution. While the system is certainly in the fast-exchange regime, the exchange process is too fast to be accurately measured by this technique. The value for k_s can be bracketed with a conservative lower boundary of $\geq 10^7$ M^{-1} s^{-1}, a value that appears to be larger than other low molecular weight copper model complexes for which similar data is available. The unusually large magnitude of k_s likely reflects the minimal structural reorganization that accompanies $Cu^1Cu^1 \leftrightarrow Cu^{1.5}Cu^{1.5}$ interchange.

Introduction

Biological electron transfer agents that feature copper are most typically mononuclear in nature, as observed in the well-known "blue copper" family of proteins.[1-3] Such systems and relevant small molecule model complexes have been studied intensively to gain an appreciation of how the inner coordination geometry of a copper ion dictates its ability to mediate rapid electron transfer.[4] While the issues that dictate electron-transfer rates in copper proteins are an ongoing topic of concern,[4a,5] it is widely accepted that structural reorganization needs to be minimized to achieve rapid rates.[6]

Higher nuclearity copper-based electron-transfer agents, while less common, are now well established. For example, a collection of spectroscopic and more recent structural data has revealed that cytochrome *c* oxidase accomplishes enhanced electron transfer (ET) into and out of a buried Cu_A site by virtue of a highly covalent, thiolate-bridged Cu_2S_2 diamond core structure type.[7,8] Among the various low molecular weight systems that have been developed to model aspects of this Cu_A site,[9-12] perhaps the most structurally relevant concerns Tol-

(1) (a) Guss, J. M.; Freeman, H. C. *J. Mol. Biol.* **1983**, *169*, 521. (b) Gray, H. B.; Malmstrom, B. G.; Williams, R. J. P. *J. Biol. Inorg. Chem.* **2000**, *5*, 551.
(2) Shibata, N.; Inoue, T.; Nagano, C.; Nishio, N.; Kohzuma, T.; Onodera, K.; Yoshizaki, F.; Sugimura, Y.; Kai, Y. *J. Biol. Chem.* **1999**, *274*, 4225.
(3) Suzuki, S.; Kataoka, K.; Yamaguchi, K.; Inoue, T.; Kai, Y. *Coord. Chem. Rev.* **1999**, *192*, 245.
(4) (a) Ambundo, E. A.; Yu, Q.; Ochrymowycz, L. A.; Rorabacher, D. B. *Inorg. Chem.* **2003**, *42*, 5267. (b) Kyritsis, P.; Dennison, C.; Ingledew, W. J.; McFarlane, W.; Sykes, A. G. *Inorg. Chem.* **1995**, *34*, 5370. (c) Groenveld, C. M.; Canters, G. W. *J. Biol. Chem.* **1988**, *263*, 167. (d) Groenveld, C. M.; Dahlin, S.; Reinhammer, B.; Canters, G. W. *J. Am. Chem. Soc.* **1987**, *109*, 3247.
(5) (a) Solomon, E. I.; LaCroix, L. B.; Randall, D. W. *Pure Appl. Chem.* **1998**, *70*, 799. (b) Randall, D. W.; Gamelin, D. R.; LaCroix, L. B.; Solomon, E. I. *J. Biol. Inorg. Chem.* **2000**, *5*, 16.

(6) Marcus, R. A.; Sutin, N. *Biochim. Biophys. Acta* **1985**, *811*, 265.
(7) (a) Ferguson-Miller, S.; Babcock, G. T. *Chem. Rev.* **1996**, *96*, 2889. (b) Gamelin, D. R.; Randall, D. W.; Hay, M. T.; Houser, R. P.; Mulder, T. C.; Canters, G. W.; de Vries, S.; Tolman, W. B.; Lu, Y.; Solomon, E. I. *J. Am. Chem. Soc.* **1998**, *120*, 5246. (c) George, S. D.; Metz, M.; Szilagyi, R. K.; Wang, H. X.; Cramer, S. P.; Lu, Y.; Tolman, W. B.; Hedman, B.; Hodgson, K. O.; Solomon, E. I. *J. Am. Chem. Soc.* **2001**, *123*, 5757. (d) Ramirez, B. E.; Malmstrom, B. G.; Winkler, J. R.; Gray, H. B. *Proc. Natl. Acad. Sci. U.S.A.* **1995**, *92*, 11949.
(8) (a) Kroneck, P. M. H.; Antholine, W. E.; Riester, J.; Zumft, W. G. *FEBS Lett.* **1989**, *248*, 212. (b) Kroneck, P. M. H.; Antholine, W. E.; Riester, J.; Zumft, W. G. *FEBS Lett.* **1988**, *242*, 70. (c) Antholine, W. E.; Kastrau, D. H. W.; Steffens, G. C. M.; Buse, G.; Sumft, W. G.; Kroneck, P. M. H. *Eur. J. Biochem.* **1992**, *209*, 875.

Scheme 1
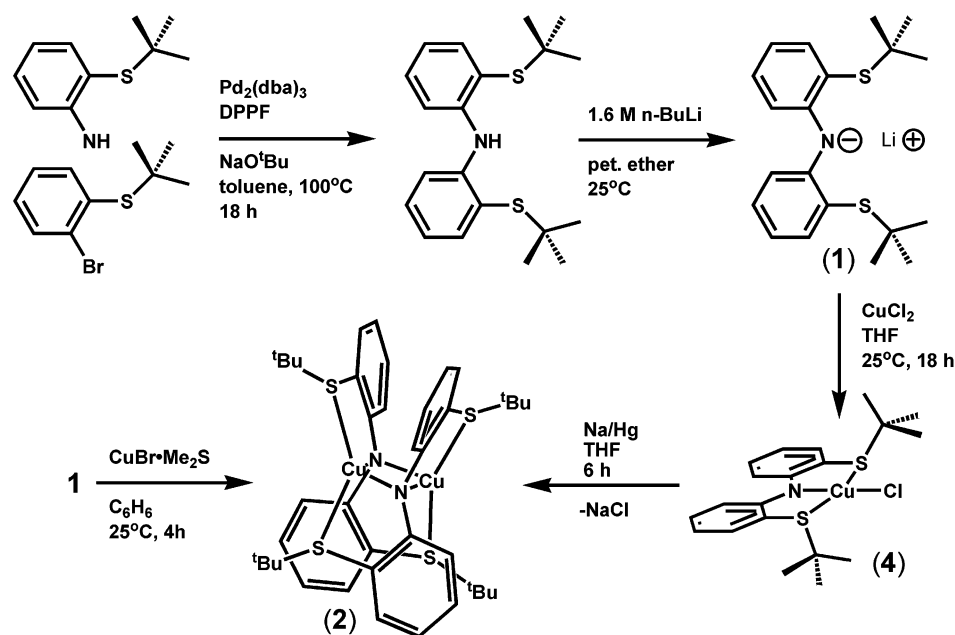
man's thiolate-bridged, mixed-valence $\{L^{N3S}Cu^{1.5}\}_2^+$ diamond core complex.[9a] This complex features an EPR signal consistent with a fully delocalized class III diamond core description,[7b,9a] as observed for the resting state form of Cu_A.[7b,8] Despite this similarity, the Cu⋯Cu distance in the Tolman model system is much larger than that observed in Cu_A, and the complex does not reproduce the reversible Cu^1Cu^1 to $Cu^{1.5}Cu^{1.5}$ redox behavior of Cu_A. Several dicopper systems that diverge from the diamond core structural motif do show reversible redox behavior for a $Cu^{1.5}Cu^{1.5}$ mixed-valence state.[11c,13] For example, a family of dicopper azacryptates has been developed that successfully bring two copper centers constrained by the azacryptate cage into much closer proximity ($\sim$2.35−2.4 Å).[13a] Some of these complexes, which are characterized by a direct metal−metal σ bond that is quite distinct from the bonding situation in Cu_A, nonetheless exhibit very rapid electron self-exchange (k_s) between their oxidized and reduced forms ($\sim$10^5 M^{-1} s^{-1}).[13b]

Yet to be developed are *diamond core* copper systems that can reversibly model *both* the reduced Cu^1Cu^1 and the delocalized $Cu^{1.5}Cu^{1.5}$ redox states observed in Cu_A.[14] Ligand systems that would help to minimize structural reorganization between these two redox forms and hold the two copper centers of a diamond core in close enough proximity to reproduce the short Cu−Cu bond distance observed in Cu_A ($\sim$2.5 Å),[15] might serve as simplified functional models for the redox behavior of

Cu_A.[7b−d] One avenue into this regime using small molecule design is to replace the thiolate bridging units inherent to the Cu_2S_2 diamond core of Cu_A with amido bridging units. Such a strategy should slide the copper centers closer together so as to better model the distance observed in Cu_A while still maintaining a Cu_2X_2 diamond core motif. Moreover, such an approach might shed some light on whether thiolate plays a unique role in facilitating rapid electron-transfer chemistry by bringing two copper centers of a diamond core into strong electronic communication. Herein we describe a Cu_2N_2 diamond core system supported by sulfur-rich, tridentate amido ligands that exhibits a fully reversible and very facile one-electron redox process between a Cu^1Cu^1 and a class III delocalized $Cu^{1.5}Cu^{1.5}$ form. Solid-state structural snapshots of both redox forms are described that reveal (i) very short Cu⋯Cu distances akin to those in Cu_A and (ii) minimal structural reorganization upon oxidation from the reduced Cu^1Cu^1 to the delocalized $Cu^{1.5}Cu^{1.5}$ state. These features facilitate very fast rates of electron self-exchange between the reduced and one-electron oxidized forms of the system ($\geq$10^7 M^{-1} s^{-1}), rates which to our knowledge are faster than those measured for other low molecular weight copper complexes.[4a,13b] A distinct Cu⋯Cu compression accompanies the one-electron oxidation process that may reflect the onset of direct Cu−Cu electronic exchange.

Results and Discussion

Palladium(0) cross-coupling of 2-*tert*-butylsulfanyl bromobenzene with 2-*tert*-butylsulfanyl aniline afforded bis(2-*tert*-butylsulfanylphenyl)amine in 87% isolated yield.[16,17] Addition of ^{n}BuLi to the purified amine provided its lithium salt,

(9) (a) Houser, R. P.; Young, V. G., Jr.; Tolman, W. B. *J. Am. Chem. Soc.* **1996**, *118*, 2101. (b) Blackburn, N. J.; de Vries, S.; Barr, M. E.; Houser, R. P.; Tolman, W. B.; Sanders, D.; Fee, J. A. *J. Am. Chem. Soc.* **1997**, *119*, 6135. (c) Hagadorn, J. R.; Zahn, T. I.; Que, L., Jr.; Tolman, W. B. *J. Chem. Soc., Dalton Trans.* **2003**, 1790.
(10) Al-Obaidi, A.; Baranovič, G.; Coyle, J.; Coates, C. G.; McGarvey, J. J.; McKee, V.; Nelson, J. *Inorg. Chem.* **1998**, *37*, 3567.
(11) (a) LeCloux, D. D.; Davydov, R.; Lippard, S. J. *Inorg. Chem.* **1998**, *37*, 6814. (b) LeCloux, D. D.; Davydov, R.; Lippard, S. J. *J. Am. Chem. Soc.* **1998**, *120*, 6810. (c) He, C.; Lippard, S. J. *Inorg. Chem.* **2000**, *39*, 5225.
(12) Gupta, R.; Zhang, Z. H.; Powell, D.; Hendrich, M. P.; Borovik, A. S. *Inorg. Chem.* **2002**, *41*, 5100.
(13) (a) Nelson J.; McKee, V.; Morgan, G. G. *Prog. Inorg. Chem.* **1998**, *47*, 167. (b) Coyle, J. L.; Elias, H.; Herlinger, E.; Lange, J.; Nelson, J. *J. Biol. Inorg. Chem.* **2001**, *6*, 285.
(14) Dicopper systems structurally distinct from the Cu_2X_2 diamond core motif have in certain cases shown a reversible $Cu^1Cu^1/Cu^{1.5}Cu^{1.5}$ redox process. See, for example, 11c and references therein.
(15) (a) Blackburn, N. J.; Barr, M. E.; Woodruff, W. H.; van der Oost, J.; de Vries, S. *Biochemistry* **1994**, *33*, 10401. (b) Williams, M.; Lapplalainen, P.; Kelly, M.; Sauer-Eriksson, E.; Saraste, M. *Proc. Natl. Acad. Sci. U.S.A.* **1995**, *92*, 11955.
(16) See related L$_2$N$^-$ ligand [bis(8-quinolinyl)amido]Li: Peters, J. C.; Harkins, S. B.; Brown, S. D.; Day, M. W. *Inorg. Chem.* **2001**, *40*, 5083.
(17) (a) Wolfe, J. P.; Tomori, H.; Sadighi, J. P.; Yin, J. J.; Buchwald, S. L. *J. Org. Chem.* **2000**, *65*, 1158. (b) Alcazar-Roman, L. M.; Hartwig, J. F.; Rheingold, A. L.; Liable-Sands, L. M.; Guzei, I. A. *J. Am. Chem. Soc.* **2000**, *122*, 4618.
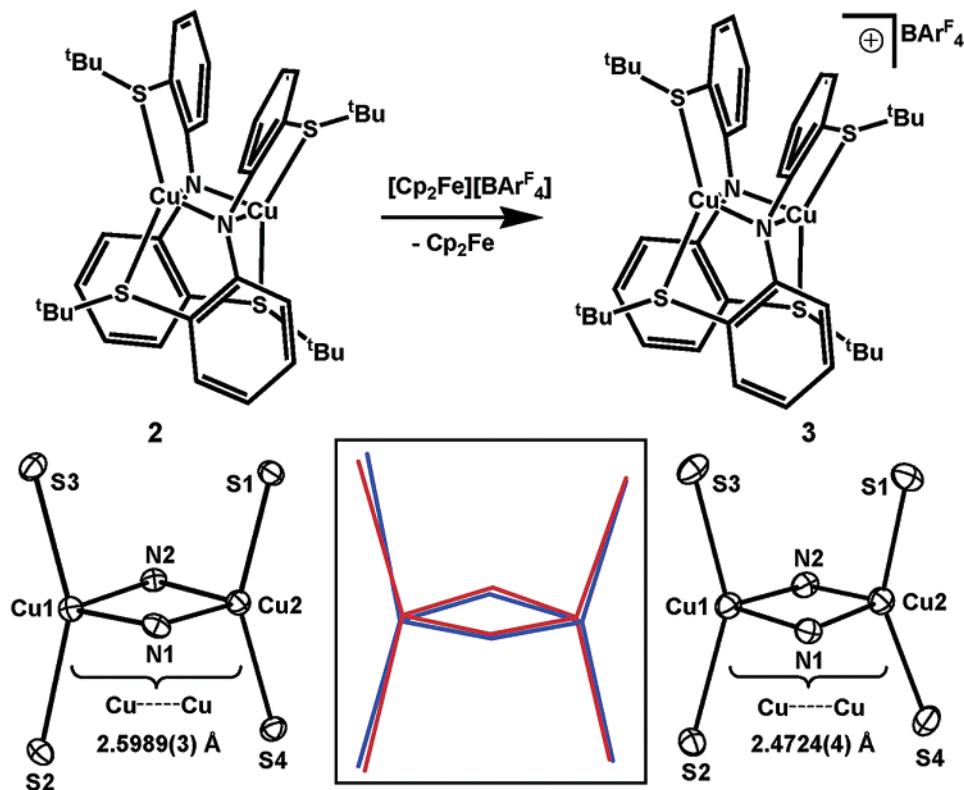
Figure 1. Molecular representations (top) of **2** and **3** (BAr^F_4 = B(3,5-(CF₃)₂C₆H₃)₄). Displacement ellipsoid representations (50%) of the core atoms of **2** (bottom left) and **3** (bottom right) and graphical overlay (center; **2** in red, **3** in blue). Selected bond lengths (Å) and angles (deg): For **2** vs **3**: Cu1−Cu2, 2.5989(3) vs 2.4724(4); Cu1−N1, 2.1149(14) vs 2.0887(16); Cu1−N2, 2.1303(14) vs 2.1011(17); Cu2−N1, 2.0850(14) vs 2.0641(16); Cu2−N2, 2.1395(14) vs 2.0568(16); Cu1−S2, 2.2730(5) vs 2.2805(6); Cu1−S3, 2.2854(5) vs 2.2805(6); Cu2−S4, 2.2735(5) vs 2.2797(6); Cu2−S1, 2.2853(5) vs 2.2834(6); Cu2−N1−Cu1, 76.45(5) vs 73.07(5); Cu1−N2−Cu2, 74.99(5) vs 72.96(5); S2−Cu1−S3, 152.921(19) vs 150.50(2); S4−Cu2−S1, 153.233(19) vs 150.71(2); N1−Cu1−N2, 103.88(5) vs 105.53(6); N2−Cu2−N1, 104.59(5) vs 108.04(5).

abbreviated as [SNS][Li] (**1**) (Scheme 1). Access to a diamagnetic dicopper(1,1) complex was accomplished by reaction of **1** with CuBr·Me₂S in benzene. Analytically pure yellow needles were obtained by recrystallization of the crude product from dichloromethane, and XRD analysis established the dimeric species {[SNS][Cu]}₂ (**2**) shown in Figure 1. Addition of a stoichiometric amount of [Cp₂Fe][B(3,5-(CF₃)₂C₆H₃)₄] to **2** produced the dinuclear complex [{[SNS][Cu]}₂][B(3,5-(CF₃)₂C₆H₃)₄] (**3**), which exhibits a temperature-independent magnetic moment between 10 and 295 K (μ_{eff} = 1.54 μ_B at 75 K (SQUID)). Analytically pure **3** was isolated as red-brown crystals by crystallization from a petroleum ether/diethyl ether mixture. Employing a Cu(II) source provided access to a mononuclear copper(II) complex supported by the [SNS] ligand scaffold. This was accomplished by stirring a slurry of **1** and CuCl₂ in THF for 18 h, after which time the square-planar copper complex [SNS]CuCl (**4**) was isolated as a deep green solid. X-ray quality crystals were obtained by recrystallization from THF/petroleum ether at −30 °C, and the solid-state structure of **4** is shown in Figure 2. Of note from the structure is the orientation of the *tert*-butyl groups, which are directed toward opposite faces of the square plane, and the canted nature of the aryl rings. These features provide the complex with molecular C_2 symmetry. The Cu−N bond distance is 1.915(2) Å, and the Cu−S1 and Cu−S2 bond distances are 2.3476(7) Å and 2.3465(7) Å, respectively. Few amido complexes of copper(II) have been prepared for comparison of the Cu−N bond distance. Perhaps the most relevant complex is [BQA]CuCl
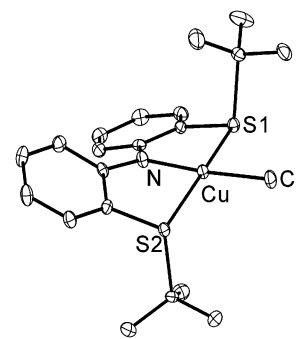

Figure 2. Solid-state molecular structure of **4** (50% displacement ellipsoids). The protons have been removed for clarity. Selected bond lengths (Å) and angles (deg): Cu−N, 1.915(2); Cu−Cl, 2.2068(7); Cu−S1, 2.3476(7); Cu−S2, 2.3465(7); N−Cu−Cl, 173.44(7); S1−Cu−S2, 167.35(3); N−Cu−S1, 86.02(6); N−Cu−S2, 86.37(6); S1−Cu−Cl, 95.89(2); S2−Cu−Cl, 92.80(2).

(BQA = bis(8-quinolinyl)amido),[18] which features a Cu−N(amido) distance of 1.935(2) Å. The Cu−S distances in **4** appear to be typical for Cu(II) based upon an analysis of data stored in the Cambridge Structural Database (CSD, av = 2.38 Å).[19] The EPR spectrum of **4**, which is shown in Figure 3, confirms its expected $S = 1/2$ spin state. The reduction of **4** by 1.05 equiv of Na/Hg amalgam in THF provides an alternative synthesis of the dicopper complex **2**.

(18) Puzas, J. P.; Nakon, R.; Petersen, J. L. *Inorg. Chem.* **1986**, *25*, 3837.
(19) Cambridge Structural Database. http://www.ccdc.cam.ac.uk/ (accessed November 2003).
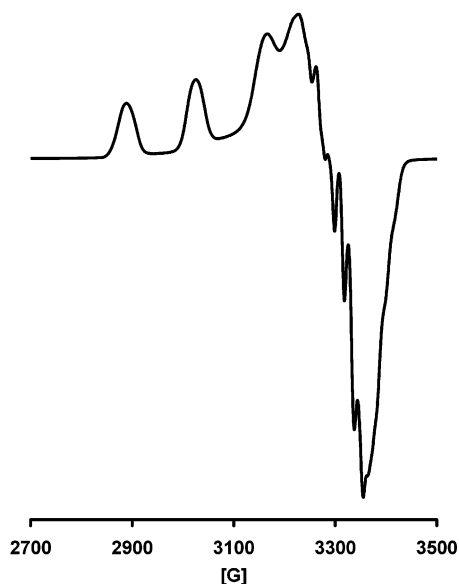
Figure 3. X-band EPR spectrum (9.40 GHz) of **4** at 77 K in 2-methyl-tetrahydrofuran.

The solid-state structures of complexes **2** and **3** are unique and of central interest. A common, dinuclear Cu_2N_2 diamond core structure type featuring anionic amido (NR_2^-) bridging units is observed for each complex (Figure 1). The four-coordinate copper centers of both **2** and **3** are quite distorted from idealized tetrahedra and are perhaps better described as cis-divacant octahedra. In this latter formulation, the thioether donors occupy the two axial sites (av S−Cu−S angle: 153° for **2**; 150.5° for **3**) and the amido bridges the two equatorial sites (av Cu−N−Cu angle: 75.8° for **2**; 73.0° for **3**). The two sulfur donors common to each amido bridge bind such that each coordinates a different copper center, thereby providing idealized D_2 symmetry to each system.[16] The distinct ligand binding motifs between structures **2** and **3** and the square-planar complex **4** underscore the coordinative flexibility of the [SNS]⁻ ligand.

The high structural similarity between the reduced and oxidized forms of **2** and **3**, clearly evident from the graphical overlay of their cores that are shown in Figure 1, is to our knowledge unprecedented in a dicopper diamond core system. Close inspection of the bond distances of the core atoms of **2** and **3** nonetheless exposes several noteworthy differences. Foremost among these is the marked shortening of the Cu···Cu distance in **3** (2.472 Å) by comparison to that of **2** (2.599 Å), a net change of ~0.13 Å. The short Cu···Cu distance observed for **3** is nearly identical to that observed for the mixed-valence form of Cu_A in cytochrome *c* oxidase.[15] The Cu−N bond distances in **3** are on average slightly shorter than in **2** (av for **3** = 2.08 Å; av for **2** = 2.12 Å), and the Cu−N−Cu angles are reduced (by approximately 2°) as the copper centers slide closer together. Interestingly, despite the contraction of the Cu_2N_2 core, the Cu−S bond distances remain effectively unchanged (the average of the Cu−S distances for both **2** and **3** is 2.28 Å).

Complex **2** exhibits a fully reversible redox process at −390 mV in CH_2Cl_2 (Fc⁺/Fc, 0.30 M [$^nBu_4N$][PF_6], 50 mV/s; Fc = ferrocene) that we assign as the $Cu^{1.5}Cu^{1.5}/Cu^1Cu^1$ redox couple (Figure 4).[20] The redox process is also reversible in THF solution at −250 mV (Fc⁺/Fc, 0.35 M [$^nBu_4N$][PF_6], 50 mV/s). An

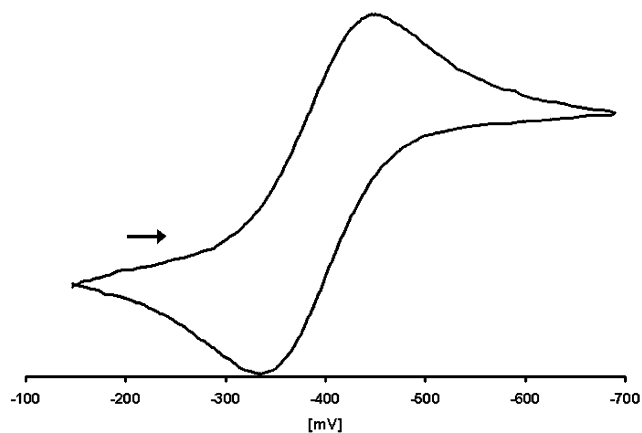**Figure 4.** Cyclic voltammetry of **2** in CH_2Cl_2 (0.30 M [$^nBu_4N$][PF_6], 50 mV/s) referenced vs Fc⁺/Fc.
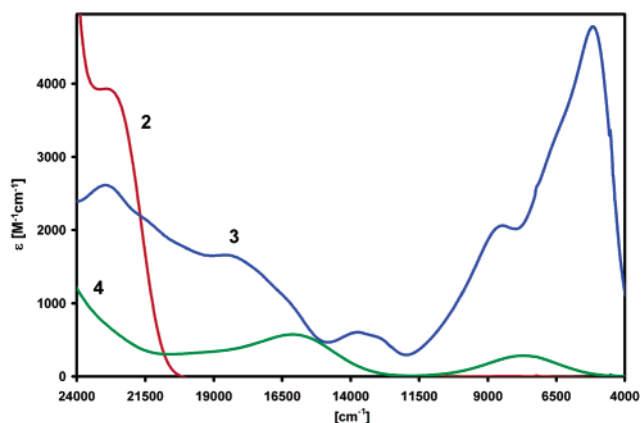

Figure 5. Electronic absorption spectrum of **2** (red), **3** (blue), and **4** (green) in methylene chloride-d_2.

irreversible redox process[21] is observed at much higher potential in CH_2Cl_2 (E_{pa} = +560 mV; see Supporting Information) and in THF ($E_{pa} \approx$ +570 mV; see Supporting Information) that most likely reflects oxidation to an unstable dicopper(II,II) species. The large difference in the anodic potentials (880 mV in CH_2Cl_2) between these waves suggests the possibility of strong stabilization of the $Cu^{1.5}Cu^{1.5}$ form due to class III delocalization. EPR data presented below supports this assertion.

The optical spectrum of yellow **2** (Figure 5) was recorded in the range between 24 000 and 4000 cm⁻¹ and shows a single, fairly intense absorption at 23 000 cm⁻¹ (ϵ = 3900 M⁻¹ cm⁻¹). The optical spectrum of **3** (Figure 5) in this range is much richer. While its spectrum is clearly unique from that obtained for Cu_A and related mixed-valence model complexes, it does contain several gross features that may be related to some of the absorption features recorded for these other systems.[7b] For example, a low energy near-IR absorption at 8550 cm⁻¹ (ϵ = 2050 M⁻¹ cm⁻¹ in CD_2Cl_2) is observed for **3** that lies slightly to the blue of a band that has been assigned as the $\Psi \rightarrow \Psi*$ transition of {$L^{N3S}Cu^{1.5}$}$_2^+$ (6760 cm⁻¹ in solution).[7b] At slightly

(20) Scaling of the $Cu^{1.5}Cu^{1.5}/Cu^1Cu^1$ redox couple to NHE provides an approximate value of +550 mV, reasonably close to the $Cu^{II}Cu^I/Cu^ICu^I$ couple measured for the Cu_A cofactor of *Thermus thermophilus* cytochrome ba_3 in water (+240 mV). See: Immoos, C.; Hill, M. G.; Sanders, D.; Fee, J. A.; Slutter, C. E.; Richards, J. H.; Gray, H. B. *J. Biol. Inorg. Chem.* **1996**, *1*, 529.
(21) The second oxidation process in dichloromethane solvent suggests the process may be modestly reversible under such conditions. See Supporting Information.

lower energy, an appreciably more intense absorption is observed (5240 cm⁻¹; $\epsilon = 4700$ M⁻¹ cm⁻¹ in CD_2Cl_2) in the spectrum for **3**, which appears to be unique from those spectra obtained for Cu$_A$ and relevant model complexes. Another intriguing band of fairly low intensity is centered around 13 400 cm⁻¹ ($\epsilon_{max} = 600$ M⁻¹ cm⁻¹). This feature appears to be a superposition of two uniquely defined absorptions. Several broad features are also evident at higher energy between 16 000 and 24 000 cm⁻¹. The optical spectrum of square-planar **4** shows two broad and relatively weak transitions, one centered at 15 000 cm⁻¹ ($\epsilon = 320$ M⁻¹ cm⁻¹) and one at 7800 cm⁻¹ ($\epsilon = 280$ M⁻¹ cm⁻¹).

For comparison, the lowest energy band of Cu$_A$, which has been assigned as the $\Psi \rightarrow \Psi^*$ transition, is observed at 13 400 cm⁻¹.[7b] The significant energy difference in the $\Psi \rightarrow \Psi^*$ transition between $\{L^{N3S}Cu^{1.5}\}_2{}^+$ and Cu$_A$ has been attributed to the significant difference in their respective Cu−Cu distances. The distance in $\{L^{N3S}Cu^{1.5}\}_2{}^+$ is 2.92 Å, and that in Cu$_A$ is ∼2.5 Å.[7b] Whereas direct Cu−Cu π overlap is possible for Cu$_A$, no direct exchange is presumably operative in $\{L^{N3S}Cu^{1.5}\}_2{}^+$ because of its much larger internuclear distance. Given these data, it would certainly be of interest to determine the origin of the bands centered at ∼13 400 cm⁻¹ for **3** or those lower energy features centered around 8600 and 5240 cm⁻¹. In particular, it is of interest to determine which of these, if any, arises from a $\Psi \rightarrow \Psi^*$ transition given that this latter complex features a Cu−Cu distance that is very similar (2.4724(4) Å) to that observed in Cu$_A$.

A geometry optimization and electronic structure calculation of **3** using DFT (JAGUAR 5.0, B3LYP/LACVP**) was performed using the crystallographically determined X-ray coordinates as the initial geometry guess.[22] The calculation provided a theoretically determined structure whose geometry agreed remarkably well with the experimental structure. The theoretically determined bond distances and angles are tabulated for comparison with the experimental structure of **3** in the Supporting Information. The electronic structure of **3** afforded by the DFT calculation suggests that the redox active singly occupied molecular orbital (SOMO) (Figure 6) contains significant orbital contributions from the four atoms of the Cu_2N_2 diamond core. The SOMO is antibonding with respect to each of the four Cu−N interactions and also the Cu−Cu interaction. This phase pattern is consistent with the observed Cu_2N_2 core expansion that occurs when this orbital becomes doubly occupied by reduction to the Cu^{1}Cu^1 species **2**. The SOMO shown in Figure 6 shows a phase relationship similar to that calculated for the SOMO of the thiolate-bridged dicopper site of Cu$_A$.[7c]

The X-band EPR spectrum of **3** was obtained in 2-methyltetrahydrofuran in the temperature range between 5 and 80 K (Figure 7). The data obtained are fully consistent with describing the system as a class III mixed-valence species. The observed EPR signal, which retains its structure from 5 to 80 K, displays seven-line hyperfine coupling due to the dicopper core, as expected for a system featuring one unpaired electron that is
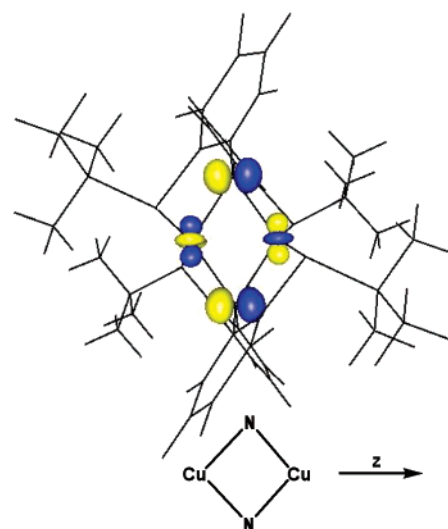
(22) Geometry optimization and electronic structure calculation (JAGUAR 5.0, B3LYP/LACVP**) were performed on the complete structure of the cation of **3** assuming a doublet ground state (no symmetry constraints applied; crystallographic coordinates of **3** were used as the HF initial guess). See Supporting Information for details. *Jaguar*, version 5.0, Schrodinger: Portland, OR, 2002.

Figure 6. DFT-minimized structure of **3** and contour plot (value = 0.065) of its singly occupied molecular orbital (SOMO).[22]
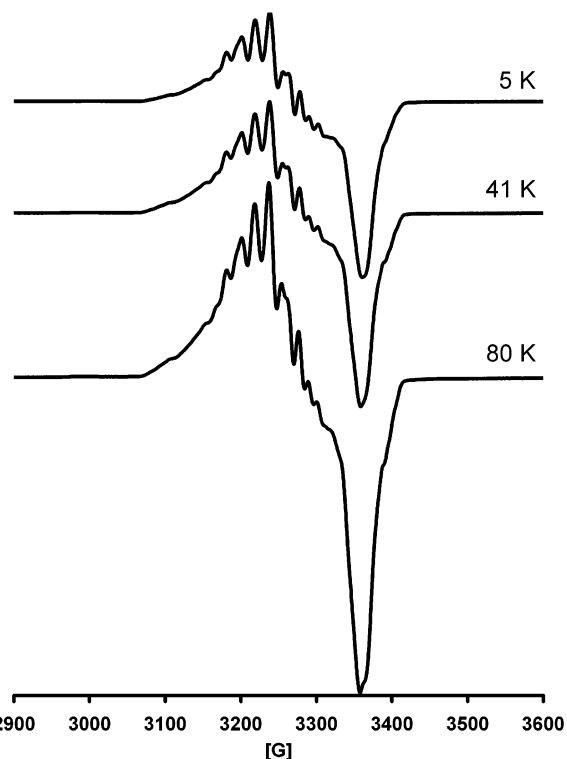

Figure 7. X-band EPR spectrum (9.38 GHz) of **3** at 80, 41, and 5 K in 2-methyltetrahydrofuran.

coupled to two copper centers. While super-hyperfine coupling to the bridging nitrogen nuclei of the Cu_2N_2 core might be anticipated, such coupling is not readily discerned in the X-band spectra. We attempted to simulate the experimental EPR spectrum for **3** acquired at 5.2 K and achieved a crude fit to the spectrum (see Supporting Information). The difficulty with simulating the spectrum does not appear to be due to a trace copper(II) impurity: the spectrum shown proved highly reproducible using samples that had been independently synthesized and recrystallized. Moreover, the EPR spectrum of complex **4** shown in Figure 3 is typical of copper(II) complexes supported by the [SNS]⁻ ligand, and similar features are not present in the spectrum of **3**. The three *g* tensors in the spectrum of **3** are

poorly resolved ($g_1 = 2.013$, $g_2 = 2.065$, $g_3 = 2.069$), and this makes the simulation difficult. Acquisition of the EPR spectrum of **3** at higher field strength should help to resolve the spectrum. The experimental EPR data and our crude simulation do nonetheless support the assignment of **3** as an $S = 1/2$ system coupled to a symmetric dicopper center.

Given the small structural reorganization that occurs upon oxidation of **2** to **3** and the reversibility of the process, we reasoned that unusually rapid intermolecular electron-transfer kinetics might be observable in the present system. Whereas electron-transfer kinetics at biological copper sites and low molecular weight copper complexes have been the subject of many previous studies,[4,13,23] in part motivated by the rapid electron-transfer rates obtained in type 1 copper sites of blue copper proteins,[4b−d] to our knowledge such studies have not included diamond core dicopper model systems. We therefore sought to measure, or at least approximate, the intermolecular self-exchange rate between **2** and **3** directly using the technique of ^1H NMR line-broadening analysis.[24]

A single and sharp resonance for the *tert*-butyl protons of **2** is observed at 1.23 ppm. For a pure sample of **2**, its line width W_2 (where line width indicates the full width at half-maximum for the Lorentzian-shaped line) is 1.3 ± 0.2 Hz. The ^1H NMR spectrum of a pure sample of **3** features a very broad resonance centered at 6.79 ppm. This resonance is slightly convoluted by overlap with the aryl protons of the $[B(3,5-(CF_3)_2C_6H_3)_4]$ counteranion. Nonetheless its line width, W_3, can be estimated as 807 ± 25 Hz. The addition of increasing amounts of cationic **3** to a solution of **2** in CD_2Cl_2 causes the observed resonance to broaden and to shift downfield. A plot of the chemical shift of this resonance as a function of the mole fraction of **2**, χ_2, reveals a linear correlation (see Supporting Information) and therefore suggests that the rate of electron exchange between **2** and **3** falls within the fast-exchange regime. If we assume a two-site exchange system composed of diamagnetic **2** and paramagnetic **3**, and if the rate law for electron transfer is first-order with respect to each reactant concentration, then eq 1 relating line widths and reactant lifetimes holds:[25,26]

$$W_{23} = \chi_3 W_3 + \chi_2 W_2 + [\chi_3 \chi_2 \{4\pi(\delta\nu)^2 k_s^{-1} C_{23}^{-1}\}] \quad (1)$$

In this equation, $\delta\nu$ represents the contact shift between **2** and **3**, k_s represents the rate constant for electron self-exchange (M^{-1} s^{-1}), and C_{23} represents the total molarity of the solution of **2** and **3**. To obtain a reliable value for k_s in the fast-exchange region, it is necessary that W_{23} be considerably larger than the sum $\{\chi_3 W_3 + \chi_2 W_2\}$. When k_s approaches very high values ($>10^8$ M^{-1} s^{-1}), the third term $[\chi_3 \chi_2 \{4\pi(\delta\nu)^2 k_s^{-1} C_{23}^{-1}\}]$ approaches zero, and W_{23} converges to the sum $\{\chi_3 W_3 + \chi_2 W_2\}$. Within the error estimated for our line width measurements W_2, W_3, and W_{23}, the magnitude of W_{23} is too close to the sum $\{\chi_3 W_3 + \chi_2 W_2\}$ to accurately determine the magnitude of k_s. In other words, small errors in our values for W_2, W_3, and W_{23} will dramatically affect the value predicted. Therefore, the rate of

the exchange process is too fast to measure accurately by the technique of NMR line-broadening analysis, and we must at present be satisfied with suggesting a conservative lower boundary limit for k_s as $\geq 10^7$ M^{-1} s^{-1}. We attempted to slow the exchange rate down by diluting the total concentration of **2** and **3**, but the line widths W_{23} obtained were still too close to the sum $\{\chi_3 W_3 + \chi_2 W_2\}$ to provide accurate values for k_s. The crude lower boundary we estimate for k_s can be compared to that measured for $Fc/[Fc][PF_6]$ by the same technique ($k_s = (4.3 \pm 0.3) \times 10^6$ M^{-1} s^{-1} at 298 K in CD_2Cl_2).[24c] More interesting is to consider values that have been measured for Cu_A for comparison. While electron self-exchange rates are obviously not available for the buried Cu_A site of cytochrome c oxidase, meaningful values for electron-transfer rates into and out of Cu_A domains have been measured. Perhaps the most meaningful value for comparison to the present model system is that determined by Slutter et al. using flash photolysis to initiate electron transfer between excited (2,2′-bipyridyl)-ruthenium(II) ($Ru(bpy)_3^{2+}$) and the soluble Cu_A domain from the cytochrome ba_3 of *Thermus thermophilus*.[27] The value estimated in that study for the second-order ET rate constant from $Ru(bpy)_3^{2+}$ to the fully oxidized Cu_A site at high ionic strength was determined to be 2.2×10^8 M^{-1} s^{-1}. Stopped flow studies with a soluble Cu_A domain and its natural partner cytochrome c_{550} from *Paracoccus denitrificans* provided rates of 1.5×10^6 M^{-1} s^{-1}.[28] Electron self-exchange values determined for the oxidized and reduced forms of plastocyanin from *Anabaena variabilis* obtained by longitudinal NMR relaxation were $1.50 \pm 0.13 \times 10^5$ M^{-1} s^{-1} at 298 K in pH 7.0 H_2O.[29] Clearly, the lower boundary for k_s we have proposed suggests our model system can achieve electron-transfer rates comparable to Cu_A. It is therefore of obvious interest to more accurately determine an ET value for the present Cu_2N_2 model system for direct comparison to a known value for a soluble Cu_A domain. Efforts are now underway to examine the flash photolysis methodology used by Slutter et al. to determine whether this will be a viable strategy.

To conclude, the amido-bridged Cu_2N_2 diamond core structures described herein provide an interesting structural departure from the thiolate-bridged diamond cores of biological Cu_A. Nonetheless, the $\{[SNS][Cu]\}_2^{+n}$ ($n = 0, 1$) system is unique among *dicopper diamond cores* in its ability to functionally model both the reduced and the one-electron oxidized mixed-valence states of biological Cu_A. Minimal structural reorganization of the $[SNS]^-$ ligand framework, and the short $Cu-Cu$ distance it supports, are likely important factors governing the reversible redox behavior of $\{[SNS][Cu]\}_2^{+n}$. Moreover, these same factors seem to provide access to a very facile $Cu^1Cu^1 \leftrightarrow Cu^{1.5}Cu^{1.5}$ electron self-exchange process ($\geq 10^7$ M^{-1} s^{-1}), the lower limit of whose magnitude is to our knowledge unprecedented in copper model complexes. These data collectively suggest that amido bridges are an attractive alternative to thiolate as a bridging unit for dicopper diamond core systems, especially if a facile electron-transfer agent is desired. Many questions remain to be answered for the dicopper systems discussed herein,

(23) Xie, B.; Elder, T.; Wilson, L. J.; Stanbury, D. M. *Inorg. Chem.* **1999**, *38*, 12.
(24) (a) Jameson, D. L.; Anand, R. *J. Chem. Educ.* **2000**, *77*, 88. (b) Nielson, R. M.; McManis, G.; Golovin, M. N.; Weaver, M. J. *J. Phys. Chem.* **1988**, *92*, 3441. (c) Yang, E. S.; Chan, M. S.; Wahl, A. C. *J. Phys. Chem.* **1980**, *84*, 3094. (d) Soper, J. D.; Mayer, J. M. *J. Am. Chem. Soc.* **2003**, *125*, 12217.
(25) Larsen, D. W.; Wahl, A. C. *J. Phys. Chem.* **1965**, *43*, 3765.
(26) Chan, M. S.; Deroos, J. B.; Wahl, A. C. *J. Phys. Chem.* **1973**, *77*, 2163.

(27) Slutter, C. E.; Langen, R.; Sanders, D.; Lawrence, S. M.; Wittung, P.; Di Bilio, A.; Hill, M. G.; Fee, J. A.; Richards, J. H.; Winkler, J. R.; Malmström, B. G. *Inorg. Chim. Acta* **1996**, *243*, 141.
(28) Lappalainen, P.; Watmough, N. J.; Greenwood, C.; Saraste, M. *Biochemistry* **1995**, *34*, 5824.
(29) Jensen, M. R.; Hansen, D. F.; Led, J. J. *J. Am. Chem. Soc.* **2002**, *124*, 4093.

Table 1. X-ray Diffraction Data for **2**, **3**, and **4**[a]

	2	3	4
chemical formula	$C_{40}H_{52}CuN_2S_4$	$C_{72}H_{64}BCu_2F_{24}N_4S_4 \cdot 1/2\ (C_4H_{10}O)$	$C_{20}H_{26}ClCuNS_2$
formula weight	816.206	1716.478	443.53
T (K)	98	100	96
λ (Å)	0.71073	0.71073	0.71073
a (Å)	10.2263(9)	10.3179(8)	17.0807(13)
b (Å)	10.6226(9)	19.3779(14)	12.3173(10)
c (Å)	19.4884(17)	19.9116(15)	19.5782(15)
α (deg)	94.017(2)	74.234(1)	90
β (deg)	90.634(2)	83.222(1)	90
γ (deg)	107.305(1)	85.603(1)	90
V (Å³)	2015.1(3)	3800.4(5)	4119.0(6)
space group	$P\bar{1}$ (No. 2)	$P\bar{1}$ (No. 2)	$Pbca$ (No. 61)
Z	2	2	8
D_{calcd} (g/cm³)	1.345	1.500	1.430
μ (mm⁻¹)	1.292	0.773	1.396
R1, wR2 ($I > 2\sigma(I)$)	0.0303, 0.0660	0.0393, 0.0810	0.0381, 0.0694

[a] $R1 = \sum||F_o| - |F_c||/\sum|F_o|$, $wR2 = \{\sum[w(F_o^2 - F_c^2)^2]/\sum[w(F_o^2)^2]\}^{1/2}$.

and future studies will probe the spectroscopy and electron-transfer kinetics of these new systems in more detail. Moreover, we will explore whether synthetic access to related Cu₂N₂ structure types using other [LNL]⁻ ligands is possible so as to probe structure−function relationships in such systems more thoroughly.

Experimental Section

General. All manipulations were carried out using standard Schlenk or glovebox techniques under a dinitrogen atmosphere. Unless otherwise noted, solvents were deoxygenated and dried by thorough sparging with N₂ gas followed by passage through an activated alumina column. Nonhalogenated solvents were tested with a standard purple solution of sodium benzophenone ketyl in tetrahydrofuran to confirm effective oxygen and moisture removal. All reagents were purchased from commercial vendors and used without further purification unless otherwise stated. 2-*tert*-Butylsulfanyl aniline,[30] [Cp₂Fe][B(3,5-(CF₃)₂C₆H₃)₄],[31] and CuCl₂·0.66 THF[32] were prepared according to literature procedures. Elemental analyses were performed by Desert Analytics, Tucson, AZ. Deuterated solvents were purchased from Cambridge Isotope Laboratories, Inc. and degassed and dried over activated 3 Å molecular sieves prior to use. A Varian Mercury-300 or INOVA-500 NMR spectrometer was used to record ¹H, ¹³C, and ¹⁹F NMR spectra at ambient temperature. ¹H chemical shifts were referenced to residual solvent. Temperature calibration of the NMR probe was accomplished using an anhydrous methanol standard. Line shape analysis of experimental NMR was performed using the Varian 6.1c software package. GC−MS data were obtained by injecting a dichloromethane solution into a Agilent 6890 GC equipped with an Agilent 5973 mass selective detector (EI). High-resolution EI mass spectroscopy was carried out by the Caltech Chemistry Mass Spectral Facility using a JEOL JMS600. UV−vis measurements were taken on a Cary 500 UV/vis/NIR spectrophotometer using a 0.1 cm quartz cell with a Teflon stopper. IR measurements were obtained with a KBr solution cell using a Bio-Rad Excalibur FTS 3000 spectrometer controlled by Bio-Rad Merlin Software (v. 2.97) set at 4 cm⁻¹ resolution. X-ray diffraction studies were carried out in the Beckman Institute Crystallographic Facility on a Bruker Smart 1000 CCD diffractometer. Table 1 shows X-ray diffraction data for **2**, **3**, and **4**.

(30) Courtin, A.; von Tobel, H. R.; Auerbach, G. *Helv. Chim. Acta* **1980**, *63*, 1412.
(31) Chávez, I.; Alvarez-Carena, A.; Molins, E.; Roig, A.; Maniukiewicz, W.; Arancibia, A.; Arancibia, V.; Brand, H.; Manríquez, J. M. *J. Organomet. Chem.* **2000**, *601*, 126.
(32) So, J. H.; Boudjouk, P. *Inorg. Chem.* **1990**, *29*, 1592. The precise number of equivalents of THF contained in this starting material was determined by microanalysis.

Magnetic Measurements. Measurements were recorded using a Quantum Designs SQUID magnetometer running MPMSR2 software (Magnetic Property Measurement System Revision 2). Data were recorded at 5000 G. Samples were suspended in the magnetometer in a clear plastic straw sealed under nitrogen with Lilly no. 4 gel caps. Loaded samples were centered within the magnetometer using the DC centering scan at 35 K and 5000 G. Data were acquired at 2−20 K (one data point every 2 K) and 20−295 K (one data point every 5 K). The magnetic susceptibility was adjusted for diamagnetic contributions using the constitutive corrections of Pascal's constants. The molar magnetic susceptibility (χ_m) was calculated by converting the calculated magnetic susceptibility (χ) obtained from the magnetometer to a molar susceptibility (using the multiplication factor {molecular weight/[sample weight*field strength]}). Curie−Weiss behavior was verified by a plot of χ_m^{-1} versus T. Effective magnetic moments were calculated using eq 2.

$$\mu_{eff} = \sqrt{7.997\chi_m T} \qquad (2)$$

EPR Measurements. X-band EPR spectra were obtained on a Bruker EMX spectrometer (controlled by Bruker Win EPR software v. 3.0) equipped with a rectangular cavity working in the TE₁₀₂ mode. Variable temperature measurements were conducted with an Oxford continuous-flow helium cryostat (temperature range 3.6−300 K). Accurate frequency values were provided by a frequency counter built into the microwave bridge. Solution spectra were acquired in 2-methyl-tetrahydrofuran. Sample preparation was performed under a dinitrogen atmosphere in an EPR tube equipped with a ground glass joint.

Electrochemistry. Electrochemical measurements were carried out in a glovebox under a dinitrogen atmosphere in a one-compartment cell using a BAS model 100/W electrochemical analyzer. A glassy carbon electrode and platinum wire were used as the working and auxiliary electrodes, respectively. The reference electrode was Ag/AgNO₃ in THF. Solutions (CH₂Cl₂) of electrolyte (0.30 M tetra-*n*-butylammonium hexafluorophosphate) and analyte were prepared in a glovebox.

Electron Self-Exchange Rate between 2 and 3. ¹H NMR spectra were acquired in CD₂Cl₂ on a Varian Inova spectrometer operating at 499.852 MHz at 303 K. The data collection parameters were as follows: 0 s relaxation delay, 5.5 μs pulse width, and an 89988.8 Hz sweep width. The samples were weighed and dissolved in 1.0 mL of CD₂Cl₂, after which each sample tube was charged with ~0.5 mL of the solution. The sample concentrations, mole fractions, and experimental values for *W* are shown in Table 2 below. The chemical shifts and line widths of the experimental spectra were obtained by Lorentzian line-fitting using the Varian 6.1c software package.

Table 2. Line-Broadening Data, Concentrations, and Mole Fractions Used To Estimate the Lower Boundary of the Self-Exchange Reaction Rate between **2** and **3** in Dichloromethane Solution[a]

	2 only	3 only	mix-A	mix-B	mix-C
χ_2	1	0	0.75 ± 0.01	0.59 ± 0.01	0.41 ± 0.01
χ_3	0	1	0.25 ± 0.01	0.41 ± 0.01	0.59 ± 0.01
total concentration (mM)			29	24	27
no. of scans	100	1000	1000	1000	1000
chemical shift (Hz)	619	3396	1314	1766	2263
W (Hz)	1.3 ± 0.2	807 ± 25	197 ± 15	314 ± 15	458 ± 15

[a] See Supporting Information for plots of (i) chemical shift versus mole fraction of **2** and (ii) W_2, W_3, and W_{23} versus χ_2.

Synthesis of 2-*tert*-Butylsulfanyl Bromobenzene. In air, 2-bromo-thiophenol (25 mL, 0.208 mol) was added dropwise to a vigorously stirred solution of *tert*-butyl alcohol (23 g, 0.312 mol), H_2O (150 mL), and concentrated H_2SO_4 (200 mL) at -10 °C. Following the addition, the reaction was allowed to come to ambient temperature and stirring was continued for 18 h, at which time diethyl ether (50 mL) was added to the reaction mixture. The organic phase was washed with 1 M Na_2CO_3 solution (100 mL) and water (3 × 100 mL) and dried over Na_2SO_4, and the solvent was removed in vacuo. The resultant cloudy oil was fractionally distilled (90 °C/0.01 mmHg), affording a colorless oil.

^{1}H NMR (300 MHz, $CDCl_3$): δ 7.64 (m, 2H, Ar-*H*), 7.24 (t, 1H, Ar-*H*), 7.15 (t, 1H, Ar-*H*), 1.32 (s, 9H, C(C*H*$_3$)$_3$). ^{13}C NMR (126 MHz, $CDCl_3$): δ 139.7, 134.4, 133.7, 132.8, 130.3, 127.5, 48.8, 31.5. GC−MS (*m/z*): 246/244[M], 190/188[M − ((CH_3)CCH_2)], 108, 109, 82, 69, 57.

Synthesis of Bis(2-*tert*-butylsulfanylphenyl)amine: A 200-mL reaction vessel equipped with a Teflon stopcock and stir bar was charged with Pd_2(dba)$_3$ (0.365 g, 0.399 mmol), bis(diphenylphosphino)-ferrocene (DPPF) (0.442 g, 0.798 mmol), and toluene (30 mL) under a dinitrogen atmosphere. The resulting solution was stirred for 5 min, after which time 2-*tert*-butylsulfanyl bromobenzene (9.77 g, 39.9 mmol), 2-*tert*-butylsulfanyl aniline (7.23 g, 39.9 mmol), and additional toluene (70 mL) were added. The subsequent addition of NaO*t*Bu (5.37 g, 55.9 mmol) resulted in a brown solution that was stirred vigorously for 18 h at 100 °C. The solution was then allowed to cool and filtered through a silica plug that was then extracted with toluene to ensure complete removal of the desired product. Concentration of the collected extracts and removal of solvent yielded a brown solid. These solids were extracted with hexanes and filtered. Purification by recrystallization from hexanes at -30 °C afforded beige crystalline blocks (11.95 g, 87%).

^{1}H NMR (300 MHz, CD_2Cl_2): δ 8.30 (s, 1H, N-*H*), 7.52 (d, 2H, Ar-*H*), 7.43 (d, 2H, Ar-*H*), 7.25 (t, 2H, Ar-*H*), 6.83 (t, 2H, Ar-*H*), 1.33 (s, 18H, C(C*H*$_3$)$_3$). ^{13}C NMR (126 MHz, $CDCl_3$): δ 145.8, 140.0, 130.2, 120.5, 120.0, 115.4, 47.9, 31.3. IR (KBr/CH_2Cl_2, cm^{-1}): 2924, 1575, 1509, 1364, 1319, 1167, 1034. HR-EI MS: calcd for $C_{20}H_{27}NS_2$: 345.1585; found: 345.1575.

Synthesis of [Li][SNS], 1. In a 250-mL flask, bis(2-*tert*-butyl-sulfanylphenyl)amine (2.5 g, 7.25 mmol) was dissolved in petroleum ether (100 mL), and a 1.6 M solution of *n*-butyllithium in hexanes (5.9 mL, 9.43 mmol) was added dropwise, with stirring at ambient temperature. A pale yellow solid began precipitating immediately, and stirring was continued for 20 min. The solids were collected on a sintered glass frit and washed with petroleum ether (3 × 30 mL). A spectroscopically pure off-white powder (2.5 g, 98%) was obtained upon drying in vacuo.

^{1}H NMR (300 MHz, C_6D_6): δ 7.52 (d, 2H, Ar-*H*), 7.34 (d, 2H, Ar-*H*), 7.15 (t, 2H, Ar-*H*), 6.68 (t, 2H, Ar-*H*), 1.11 (s, 18H, C(C*H*$_3$)$_3$). ^{13}C NMR (126 MHz, C_6D_6): δ 164.7, 139.5, 131.0, 123.7, 121.7, 117.3, 47.4, 31.5.

Synthesis of {[SNS]Cu}$_2$, 2. A solution of **1** (800 mg, 2.28 mmol) in benzene (20 mL) was added dropwise with stirring to a suspension of CuBr·Me$_2$S (469 mg, 2.28 mmol) in benzene (40 mL). The solution

immediately became bright yellow. After 4 h, the reaction mixture was filtered through a pad of Celite on a sintered glass frit, and the solvent was removed in vacuo. The yellow solids were washed with petroleum ether (3 × 50 mL) and dried thoroughly, which afforded spectroscopically pure product (850 mg, 91%). This complex decomposes photolytically over time; and therefore, efforts were made to minimize light exposure during synthesis and storage. Analytically pure product was obtained as fine yellow crystalline needles by cooling a methylene chloride solution at -35 °C.

^{1}H NMR (300 MHz, CD_2Cl_2): δ 7.32 (d, 2H, Ar-*H*), 7.06 (t, 2H, Ar-*H*), 6.91 (d, 2H, Ar-*H*), 6.57 (t, 2H, Ar-*H*), 1.23 (s, 18H, C(C*H*$_3$)$_3$). ^{13}C NMR (126 MHz, CD_2Cl_2): δ 160.8, 136.3, 130.3, 122.9, 121.4, 116.3, 49.8, 31.1. UV−vis−NIR (CD_2Cl_2, nm (M^{-1} cm^{-1})): 426 (4000). IR (KBr pellet, cm^{-1}): 3045 (w), 2959 (m), 2921 (w), 1573 (s), 1543 (m), 1451 (s), 1428 (s), 1362 (m), 1312 (s), 1268 (m), 1154 (s), 1123 (w), 1031 (m), 818 (w), 743 (s), 725 (m). Anal. Calcd for $C_{40}H_{52}Cu_2N_2S_4$: C, 58.86; H, 6.42; N, 3.43. Found: C, 58.46; H, 6.22; N, 3.28.

Synthesis of [{(SNS)Cu}$_2$][B(3,5-(CF$_3$)$_2$C$_6$H$_3$)], 3. In a 20-mL reaction vessel equipped with a Teflon stirbar, **2** (150.0 mg, 0.184 mmol) was suspended in diethyl ether (15 mL), and [Cp$_2$Fe][B(3,5-(CF$_3$)$_2$C$_6$H$_3$)$_4$] (192.8 mg, 0.184 mmol) was added as a solid in one portion. The green reaction mixture gradually became red-brown. After 90 min, the solution was filtered through glass wool, and the filtrate was dried in vacuo. The solids were extracted with petroleum ether (3 × 30 mL) to remove the ferrocene byproduct, and drying under reduced pressure afforded the desired product as a burgundy solid (290 mg, 94%). Analytically pure material was obtained by recrystallization from layering a diethyl ether solution with petroleum ether.

^{19}F NMR (282 MHz, CD_2Cl_2): -60.19 (s, Ar-C*F*$_3$). IR (KBr pellet, cm^{-1}): 3293 (w), 3053 (w), 2968 (m), 1609 (m), 1578 (m), 1499, (m), 1454 (s), 1355 (s), 1279 (s), 1133 (br s), 887 (m), 835, (m), 756 (m), 756 (m), 714 (m), 670 (m). UV−vis−NIR (CD_2Cl_2, nm (M^{-1} cm^{-1})): 426(2500), 527(1650), 716(590), 1165(2050), 1920(4800). SQUID (solid, average 10−295 K): 1.52 μ_B ($R^2 = 0.9991$). Anal. Calcd for $C_{72}H_{64}BCu_2F_{24}N_2S_4$: C, 51.49; H, 3.84; N, 1.67. Found: C, 51.63; H, 3.80; N, 2.00.

Synthesis of (SNS)CuCl, 4. In a 50-mL round-bottom flask equipped with a Teflon stirbar, CuCl·0.66 THF (1.00 g, 5.50 mmol) was suspended in THF (30 mL), and **2** (1.93 g, 5.50 mmol) was added portionwise, immediately affording a forest green solution. The reaction mixture was stirred for 18 h at ambient temperature, and the solvent was removed in vacuo. The resultant solid was triturated with benzene (2 × 10 mL), extracted into benzene, filtered through Celite, and dried thoroughly under reduced pressure to afford **4** (2.30 g, 94%). Analytically pure material was obtained by recrystallization from THF/petroleum ether solution at -30 °C.

IR (KBr pellet, cm^{-1}): 3056 (w), 2961 (w), 1573, (m), 1456 (s), 1431 (m), 1365 (m), 1321 (s), 1240 (w), 1155 (m), 1032 (w), 767 (w), 750 (m), 740 (m). UV−vis−NIR (CD_2Cl_2, nm (M^{-1} cm^{-1})): 606 (600), 1280 (280). Anal. Calcd for $C_{20}H_{26}ClCuNS_2$: C, 54.16; H, 5.91; N, 3.16. Found: C, 54.22; H, 5.84; N, 3.08.

Reduction of 4 to 2. An amalgam of sodium (14.3 mg, 0.622 mmol) in mercury (11.1 g, 55.3 mmol) was prepared in a 20-mL reaction

vessel, and a solution of **4** (263 mg, 0.592 mmol) in THF (10 mL) was added. The reaction mixture was vigorously stirred for 6 h, filtered through Celite, and dried in vacuo. The yellow solid was extracted into benzene (20 mL), lyophilized, and washed with cold petroleum ether to afford spectroscopically pure **2** (188 mg, 78%).

Supporting Information Available: Complete crystallographic details (CIF). Details for DFT calculations and SQUID magnetization data for **3** (PDF). This material is available free of charge via the Internet at http://pubs.acs.org.

JA037364M